



Full Text View

Volume 32, Issue 5 (May 2002)

Journal of Physical Oceanography

Article: pp. 1404–1429 | [Abstract](#) | [PDF \(4.19M\)](#)

Effects of the Indonesian Throughflow on the Pacific and Indian Oceans

Tong Lee, Ichiro Fukumori, Dimitris Menemenlis, Zhangfan Xing, and Lee-Lueng Fu

Jet Propulsion Laboratory, California Institute of Technology, Pasadena, California

(Manuscript received August 24, 2000, in final form September 21, 2001)

DOI: 10.1175/1520-0485(2002)032<1404:EOTITO>2.0.CO;2

ABSTRACT

Effects of the Indonesian Throughflow (ITF) on the circulation and thermal structure of the Pacific and Indian Oceans are studied by comparing solutions of a near-global ocean general circulation model with open and closed Indonesian passages from 1981 to 1997.

The ITF contributes to the maintenance of the model circulation system around eastern Australia and the southern Indian Ocean. Blockage of the ITF weakens the Indian Ocean South Equatorial Current and Agulhas Current and strengthens the East Australian Current. The ITF does not affect the Mindanao Current, but drains waters carried by this current into the Indian Ocean and thus reduces tropical–subtropical exchange in the North Pacific. Meanwhile, it helps maintain a stronger New Guinea Coastal Undercurrent and thus enhances tropical–subtropical exchange in the south. Water parcels traveling along the western boundary of the South Pacific cross the equator in the presence of the ITF but are confined to the Southern Hemisphere without the ITF. The southern “exchange window” in which subducted waters can reach the Tropics is wider with than without the ITF. Some parcels from the southern subtropics can reach the Tropics with open ITF, but recirculate back to the subtropical gyre when the ITF is closed. These “excess” recirculated parcels reach several degrees farther south and outcrop north of Tasmania. The consequence on sea surface temperature (SST) there may have an important implication to the local climate. Blockage of the ITF depresses the mean thermocline of the tropical Pacific, increases SST in the central to eastern equatorial Pacific, and thus reduces the SST difference between the warm pool and cold tongue. It also raises the mean thermocline of the Indian Ocean (especially the southern Indian Ocean) and decreases SST in the southern Indian Ocean.

Blockage of the ITF reduces seasonal-to-interannual thermocline fluctuations in the central to eastern equatorial Pacific because the resulting deeper thermocline attenuates fluctuations in response to local Ekman pumping. The

Table of Contents:

- [Introduction](#)
- [Model configuration and](#)
- [The control run](#)
- [Effects of ITF on circulation](#)
- [Summary and conclusions](#)
- [REFERENCES](#)
- [APPENDIX](#)
- [FIGURES](#)

Options:

- [Create Reference](#)
- [Email this Article](#)
- [Add to MyArchive](#)
- [Search AMS Glossary](#)

Search CrossRef for:

- [Articles Citing This Article](#)

Search Google Scholar for:

- [Tong Lee](#)
- [Ichiro Fukumori](#)
- [Dimitris Menemenlis](#)
- [Zhangfan Xing](#)
- [Lee-Lueng Fu](#)

opposite is true in the southern Indian Ocean for the interannual timescale. However, seasonal thermocline fluctuation in that area is weakened when the ITF is blocked (despite a shallower thermocline). It indicates that local Ekman pumping is not the dominant mechanism controlling seasonal thermocline variability there as previously suggested. Radiation of planetary waves from the ITF area and advection by the ITF-dependent South Equatorial Current could also be important. Blockage of the ITF also reduces interannual variability of SST in the eastern equatorial Pacific and enhances those in the tropical southern Indian Ocean and south of Tasmania.

The results indicate that the ITF may affect El Niño–Southern Oscillation by modifying tropical–subtropical exchanges, mean tropical thermocline structure, mean SST difference between the warm pool and cold tongue, and seasonal-to-interannual variabilities of thermocline depth and SST.

1. Introduction

The Indonesian Throughflow (ITF) is widely known, on average, to carry warm and fresh Pacific waters through the Indonesian archipelago into the Indian Ocean. It is the only channel in the Tropics through which interocean exchange of water masses occurs. [Gordon \(1986\)](#) suggested that the ITF could be important to global ocean thermohaline circulation as it might return the North Atlantic Deep Water that upwelled and warmed in the Pacific back to the Atlantic. [Godfrey \(1996\)](#) discussed several aspects of ITF effects on the Pacific and Indian Ocean circulation and discussed the important impact on surface heat flux. The potential role of the ITF to the global climate system remains to be an important area of investigation.

Measuring the total transport of the ITF is difficult due to the complicated geometry in the region with many passages and because of the large variability of transport through various passages. [Godfrey \(1996\)](#), in his comprehensive review of ITF-related studies, discussed some of the difficulties in estimating the ITF using various methods. The estimates of total and partial ITF transports from various direct and indirect measurements roughly range from somewhat below zero (from the Indian into the Pacific Oceans) to nearly 20 Sv ($\text{Sv} \equiv 10^6 \text{ m}^3 \text{ s}^{-1}$) into the Indian Ocean. Based on a linear inversion from global hydrographic sections using conservation principles, [Macdonald \(1998\)](#) obtained an estimated mean ITF transport of 10 ± 10 Sv, which is consistent with the mean and uncertainty of various measurements. Uncertainties in estimating ITF transport cast a major difficulty in understanding physical processes associated with the ITF. Two major issues related to studies of the ITF are mechanisms controlling the mean and variability of the ITF (in terms of its transport and structure) and effects of the ITF on ocean circulation and the coupled ocean–atmosphere system on various timescales. This study focuses on the latter issue.

There have been a number of numerical modeling studies evaluating effects of the ITF on the circulation of the Pacific and Indian Oceans and on the global climate system, mostly by comparing model solutions with open and closed Indonesian passages. These modeling studies are briefly reviewed below.

Based on a global ocean general circulation model (OGCM) that has relatively coarse resolution forced by climatological mean surface forcings that is constant in time, [Hirst and Godfrey \(1993\)](#), hereafter HG) discussed the effects of the ITF on the mean state of the Pacific and Indian Oceans by examining equilibrium model solutions with and without the ITF. The ITF is found to have an overall effect of cooling the Pacific and warming the Indian Ocean. Large changes in sea surface temperature (SST) and thus surface heat flux are found in several regions such as the Agulhas outflow and Leeuwin Current regions in the Indian Ocean and the equatorial region and Tasmanian Sea in the Pacific. The ITF is also found to strengthen the South Equatorial Current (SEC) and Agulhas Current in the Indian Ocean, and to weaken the East Australian Current (EAC) in the South Pacific.

[Verschell et al. \(1995\)](#) used a single-layer reduced-gravity model forced by time-dependent wind during 1980–89 to study the effects of ITF on the mean as well as low- and high-frequency (longer and shorter than 6 months) variability of upper-layer thickness (a proxy for thermocline depth) in the Pacific and Indian Oceans. Changes in the southern Indian Ocean are found to be much larger than those in the Pacific Ocean. [Murtugudde et al. \(1998\)](#) used a multilayer reduced-gravity primitive equation model integrated over the period from 1980 to 1995 to address the effects of the ITF on seasonal and interannual variabilities of SST and thermocline depth of the tropical Indo–Pacific Oceans. This study also included an atmospheric mixed layer model aiming to account for some feedback of the atmosphere to SST. SST variability in the central to eastern equatorial Pacific was not correlated with ITF transport in their model, only the difference in SST variability with and without the ITF was. [Rodgers et al. \(1999\)](#), using a primitive equation OGCM for the Indo–Pacific domain driven by seasonal forcings, found that the mixing ratio of thermocline waters in the equatorial Pacific with those from the Northern and Southern Hemispheres was dependent on ITF transport.

The only modeling study that examines the effects of the ITF in a coupled ocean–atmosphere context is that by [Schneider \(1998\)](#), in which changes in SST due to blockage of the ITF, and subsequent changes in heat flux and wind, as well as the feedback into the ocean were discussed. He concluded that the ITF would affect the climate of the entire Tropics as well as part of the midlatitudes. However, model limitations limited the confidence in the sign of the feedback. Moreover, the short-

integration time precluded an analysis of effects on interannual variability.

Although some aspects of ITF effects on the Pacific and Indian Oceans have been discussed by the previous studies, many issues need further investigation, especially those related to effects on the equatorial Pacific, tropical–subtropical exchanges, and seasonal-to-interannual variability. The objectives of this study are 1) to revisit the effects of the ITF on the mean circulation and thermal structure of the Pacific and Indian Oceans, 2) to evaluate the ITF effects on seasonal-to-interannual variability, and 3) to examine its impact on tropical–subtropical exchanges. To achieve these objectives, we employed a state-of-the-art OGCM integrated over the period of 1980–97. Model solutions with open and closed Indonesian passages are compared to highlight effects of the ITF.

This study goes beyond previous related efforts in many aspects. The period of study is longer and includes the most recent El Niño. The meridional and vertical resolutions are overall higher. The higher resolution, along with the advanced mixing schemes and relatively high-frequency forcings, improve the fidelity of the model simulation. Our analysis isolates ITF effects on seasonal and interannual timescales. As will be seen, this helps shed light on the similarity and difference in forcing mechanisms of seasonal and interannual variabilities in the Pacific and Indian Oceans. Furthermore, ITF effects on tropical–subtropical exchanges is investigated.

In the next section, model configuration and numerical experiments are described. In [section 3](#), the performance of the model (with open Indonesian passages) are evaluated through comparisons with various observations and with other model simulations. The two model solutions, with open and closed passages, are compared in [section 4](#) to highlight effects of the ITF on the mean state ([section 4a](#)) and on seasonal and interannual variabilities ([section 4b](#)). Dominant processes responsible for the changes are discussed. The findings are summarized in [section 5](#).

Although blockage of the ITF creates an unrealistic oceanic state, it helps understand the influence of the ITF in maintaining the mean and controlling the variability of circulation and thermal structure in the Pacific and Indian Oceans. Describing the role of the presence of the ITF and discussing effects of blocking the ITF are philosophically the same. Moreover, comparison of model solutions with and without the ITF helps identify possible errors in the mean state and variability of regional models that ignore the ITF.

2. Model configuration and experiments

The model used is the parallel version of the primitive-equation Massachusetts Institute of Technology (MIT) OGCM ([Marshall et al. 1997a,b](#)). The spatial domain is nearly global (75°S–75°N). The model has a uniform zonal resolution of 1°. The meridional resolution is 0.3° in the Tropics (within 10° of the equator), 1° in the extratropics (poleward of 22°S and 22°N), with gradual transition in between. There are 46 vertical levels with a thickness of 10 m in the upper 150 m, gradually increasing to 400 m at depth. The meridional and vertical resolutions in the Tropics are chosen to ensure a reasonable representation of tropical currents and related thermal structure.

The model topography is shown in [Fig. 1](#) along with an enlargement near the Indonesian archipelago. It is bin-averaged from the U.S. Navy's ETOPO5 5-min world bathymetry. The major passages of the ITF are marked in the lower panel: the westernmost Lomok Strait (near 116°E), Flores Strait (near 120°E), Savu Strait (near 123°E), and the easternmost Timor Passage. Two small gaps near 6°S, 106°E and 10°S, 143°E are very shallow and carry little throughflow. Apart from bin-averaging from the high-resolution bathymetric map, no subjective artificial treatment is applied to the topography in this area. The sill depths for some major straits and passage ways are: 100 m for Lomok Strait, 423 m for Savu Strait, 1520 m for Timor Passage, 497 m for Makassar Strait, and 1520 m for Molucca Strait. The maximum sill depth for the model ITF is thus 1520 m.

The model employs two advanced mixing schemes: the so-called K-profile parameterization (KPP) vertical mixing ([Large et al. 1994](#)) and the GM–Redi isopycnal mixing ([Redi 1982](#); [Gent and McWilliams 1990](#)). The KPP scheme parameterizes convection and wind-driven vertical mixing in the surface boundary layer by specifying profiles of vertical diffusivities. In addition, a nonlocal transport term permits the transfer of surface properties to the bottom of the boundary layer during convection events. The scheme thus facilitates vertical penetration of heat and momentum near the surface, which would otherwise be too small with, for example, the traditional Pacanowski and Philander vertical mixing ([Pacanowski and Philander 1981](#)) or constant-mixing scheme. Another important feature of KPP, particularly important for equatorial currents, is the inclusion of a gradient-Richardson-mixing term that represents shear instability mixing below the surface boundary layer. Without this term, the Equatorial Undercurrent (EUC) in the Pacific would tend to be too shallow and too strong. The GM–Redi isopycnal mixing is considered more realistic than a simple constant horizontal mixing formulation because the former tends to “mix” along isopycnals and to preserve the volume of a specific water mass between any two isopycnal surfaces. In regions of steep isopycnal slope, the GM–Redi mixing coefficients are tapered following the procedure described by [Large et al. \(1997\)](#).

The model is forced at the surface by wind stress as well as heat and freshwater fluxes. Zonal and meridional wind stresses are obtained from the reanalysis product of the National Centers for Environmental Prediction (NCEP: [Kalnay et al.](#)

1996). The heat flux is a blended product with the temporal mean obtained from the Comprehensive Ocean–Atmosphere Data Set (COADS: [da Silva et al. 1994](#)) and the temporal variability from NCEP reanalysis. The “global” mean within the model domain, about 29 W m^{-2} , is removed from every grid point to minimize climate drift. In addition to this imposed heat flux, model SST is relaxed to NCEP’s SST with a spatially dependent and seasonally varying coefficient computed from the NCEP reanalysis product in the manner described by [Barnier et al. \(1995\)](#). The computed relaxation coefficients correspond to timescales of typically 30–45 days for low- and midlatitude and shorter for high-latitude oceans. The actual relaxation coefficient, in the unit of heat flux, is equal to $H/\tau \times C_p \times \rho_0$ where H is the top-layer thickness of the model (10 m), τ is the relaxation time scale, C_p is the heat capacity coefficient ($4180 \text{ J kg}^{-1} \text{ }^\circ\text{C}^{-1}$), and ρ_0 is the mean density (1000 Kg m^{-3}). The typical relaxation coefficient is thus approximately $16 \text{ W m}^{-2} \text{ }^\circ\text{C}^{-1}$. A similar treatment is applied for the freshwater flux where the imposed flux consists of temporal mean from COADS with the global mean ($7.7 \times 10^{-7} \text{ kg m}^{-2} \text{ s}^{-1}$) removed, temporal variability from the NCEP reanalysis, and relaxation to the Levitus 98 climatological mean salinity ([Boyer and Levitus 1997](#)) with a timescale of 2 months. The wind stress used has a 12-h interval. That of heat and freshwater fluxes is daily.

The model was first spun up for 10 years from rest with the Levitus 98 climatological temperature and salinity, forced by seasonal climatological forcings averaged from 1980 to 1997. The 10-yr spinup time is much shorter than thermocline timescales for mid- and high-latitude oceans, but is relatively sufficient for the development of circulation systems in upper tropical oceans, which is the main focus of the present study. The relatively short spinup time alleviates the drift of density structure in the deep ocean (a common problem for ocean models) without using relaxation of deep density to climatology, which sacrifices model dynamics. The short spinup and real-time integration period precludes the analysis of ITF effect on global ocean circulation, which involves the possible connection with upwelled North Atlantic Deep Water (i.e., the hypothesis of [Gordon 1986](#)).

Following the spinup, two integrations are performed with forcings from 1980 to 1997, with the Indonesian passages open and closed, respectively. A similar strategy was adopted by [Murtugudde et al. \(1998\)](#) in which the open and closed ITF experiments were based on the same initial conditions.


3. The control run

Before discussing effects of the ITF, we first evaluate the performance of the model based on comparisons of the control run (with open Indonesian passages) with various observations and other model simulations. [Figure 2](#) shows the spatial distribution of temporal correlation of model sea level with that obtained by the TOPEX/Poseidon satellite altimeter from 1993 to 1997. Model sea level anomalies are interpolated to the satellite tracks to facilitate the computation of correlation. Black areas indicate missing data. Reasonably good model–data correlation is seen in the tropical Pacific and Indian Oceans, especially along the equatorial wave guide, the intertropical convergence zone, and South Pacific convergence zone in the Pacific, and along 10°S and off Java in the Indian Oceans. These are areas of active wave activities (equatorial Kelvin waves, Rossby waves, coastal Kelvin waves). The good correlation in the Tropics is encouraging because it is the focus of the present study. The model underestimates the magnitude of observed variability by approximately a factor of 2 (upon global average), primarily due to limited spatial resolution and accuracies of the forcing fields.



Model temperature in the upper tropical Pacific is compared with data obtained from the 75 Tropical Ocean and Global Atmosphere (TOGA)–Tropical Atmosphere–Ocean Array (TAO) temperature moorings from 1983 to 1997. [Figure 3](#) shows the comparison of vertical profiles for (a) temporal average, (b) temporal variability, and (c) model–data correlation. The model’s stratification is too strong compared to the data. There is a cold bias in the model below the surface layer (primarily in the central to eastern equatorial Pacific). A sensitivity experiment (not shown) with a background (interior) vertical diffusivity that is four times as large ($10^{-5} \text{ m}^2 \text{ s}^{-1}$ as opposed to $2.5 \times 10^{-6} \text{ m}^2 \text{ s}^{-1}$) results in opposite differences (very diffusive thermocline and a warm bias in the upper tropical Pacific). The findings of the present study are not affected by these differences because results of a previous analysis of ITF effects based on model solutions with the large background vertical diffusivity are very similar to the findings reported in this paper. The model’s rms variability is close to the observed magnitudes in the upper 50 m, but is generally weaker than the observed value by 30%–50% farther down. The temporal correlation with the data is approximately 0.7 near the surface and the thermocline (between 100 and 150 m), and smaller at other depths.


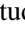
Model–data comparisons of zonal velocities at three TAO current meter mooring locations along the equatorial Pacific are presented in [Fig. 4](#). The strength of the model’s EUC is close to the observed magnitude in the western to central equatorial region (165°E and 140°W), but weaker in the eastern part (110°W). The depth of EUC core is consistent with observations. Magnitudes of the temporal rms variability of zonal velocity is about 20%–60% weaker than the observations depending on location and depth. Spatial resolution, values of background viscosity, and strength of wind forcing are believed to be the primary factors contributing to the weaker variability of the simulated velocity.

[Figure 5a](#) shows 10-day averages of simulated total ITF transport as a function of time. ITF transport is defined here

as the sum of depth-integrated transports through various passages (negative being from the Pacific to the Indian Oceans). The mean transport over this period is approximately 13 Sv. The partition among various straits from east to west are 4.3 Sv for Timor Passage, 6.5 for Savu Strait, 0.4 Sv for Flores Strait, and 1.8 Sv for Lomok Strait (cf. [Fig. 1b](#) ). Most of the transport is accounted for by the two passages in the east. That for Lomok Strait is in good agreement with current meter measurements in this strait ([Murray and Arief 1988](#)). The relative transports simulated by the model through various passages is qualitatively consistent with the general perception of how the ITF is partitioned. The vertical structure of transport through various passages is presented in [appendix A](#).

The mean value of our simulated ITF transport is well within the range of estimates inferred from various measurements, but higher than the average. It is also smaller than that simulated by OGCM of [HG](#), close to that simulated by the coupled model of [Schneider and Barnett \(1997\)](#), and larger than those simulated by reduced-gravity models of [Verschell et al. \(1995\)](#) and [Murtugudde et al. \(1998\)](#). Note that none of these models include tidal mixing near the Indonesian archipelago, which could modify ITF transport and property ([Field and Gordon 1992](#); [Takaki et al. 1996](#)). [Murtugudde et al. \(1998\)](#) applied enhanced horizontal mixing to reduce ITF transport because enhanced vertical mixing actually increased ITF transport slightly. In contrast, [Schiller et al. \(1998\)](#) was able to reduce ITF transport (slightly) through enhanced vertical mixing and improved the realism of the surface heat fluxes. The response of these two models to enhanced vertical mixing is different not only in terms of ITF transport, but in terms of the thermohaline structure as well.

The simulated ITF transport displays relatively large variability with a range and standard deviation of approximately 20 Sv and 3.5 Sv. The frequency spectrum of the ITF transport ([Fig. 5b](#) ) indicates that the dominant variability is at the annual period. Interannual and semiannual signals are also evident. The averaged seasonal cycle ([Fig. 6a](#) ) has a peak-to-trough range of approximately 7 Sv with the weakest and strongest ITF occurring in January–February and July–August, respectively. The “zigzag” in the averaged seasonal transport reflects the contribution of semiannual signal (from the Indian Ocean). The simulated seasonal variation is qualitatively consistent with that estimated by [Meyers \(1996\)](#) from XBT data and those simulated by [Masumoto and Yamagata \(1996\)](#) and [Murtugudde et al. \(1998\)](#).

The interannual anomaly of annual-mean ITF transport is shown in [Fig. 6b](#)  (solid curve) along with the model's annual-mean Niño-3 and Niño-4 SST indices (dashed and dashdotted curves). The two indices are defined as the interannual anomaly of SST averaged over the areas of (5°N–5°S, 150°–90°W) and (5°N–5°S, 160°E–150°W), respectively. The correlation between interannual ITF transport and SST anomaly is 0.47 for Niño-3 and 0.58 for Niño-4, which are above the 95% confidence level of 0.4 and 0.43. [Meyers \(1996\)](#) estimated ITF transport in the top 400 m based on geostrophic calculation using repeated XBT transects across the Indian–Ocean side of the ITF (Sunda Strait to Fremantle) over the period from 1983 to 1994. He found a relatively strong ENSO signal (a range of 5 Sv) that showed a good (anti-) correlation with the Southern Oscillation index (which is anticorrelated with the Niño-3 index). In particular, the ITF is found to be stronger during the 1988–89 La Niña and weaker during the El Niño during 1986–87 and 1991–94. Our result ([Fig. 6b](#) ) is consistent with that of [Meyers \(1996\)](#), but with smaller magnitude. Moreover, we also find relatively weak ITF during the El Niño of 1982–83 and 1997–98, which are not covered by Meyers' study period.

The above model–data comparisons indicate that the model has a reasonable performance in simulating many aspects of the circulation in the tropical Pacific and Indian Oceans as well as the transport of ITF that connects the two.

4. Effects of ITF on circulation and thermal structure

In this section, effects of the ITF on the circulation and thermal structure of the Indo–Pacific Oceans are analyzed by comparing model solutions with open and closed Indonesian passages. The two subsections address ITF effects on the mean state and seasonal-to-interannual variabilities, respectively. The comparisons are based on the temporal mean and variability of the two model solutions for the period from 1981 to 1997. The year of 1980 was excluded from the analysis because relatively large transient adjustments occur in this year following blockage of the ITF. After this year, a smaller and relatively linear trend is seen in the solution with blockage of the ITF, with the trend in velocity field being smaller than that in thermal fields.

The time-mean quantities presented in the next subsection are referred to temporal averages from 1981 to 1997. Due to a small and relatively linear trend in the solution with blockage of the ITF, the difference in time-mean state between two solutions (with and without the ITF) is somewhat larger for the later part of the integration than it is for the earlier part. For the analysis of variability, trends in both solutions are removed because the focus of variability is on seasonal-to-interannual variability. The blockage of the ITF may create low-frequency waves which could remain the solution for longer than a year. However, this effect seems small because results of an analysis based on 1990–97 are fairly similar to those presented in the following (based on 1981–97).

a. Effects on the mean state

1) MEAN CIRCULATION

Effects of the ITF on the depth-averaged circulation is illustrated by the time-mean barotropic transport stream functions with and without ITF and their differences (Fig. 7). The absence of the ITF causes an anticyclonic circulation loop around Australia and the southern Indian Ocean. This circulation extends from the Indonesian seas, southward down the east coast of Australia, westward along the northern flank of the Antarctic Circumpolar Current to the Agulhas retroflexion region, northward along the east African coast to Mozambique, then eastward across the Indian Ocean near 10°S, and back to the Indonesian seas. There is even a small extension of the loop into the south Atlantic Ocean. This change is very similar to that reported by HG except that the magnitude of the change is smaller here (due to a weaker ITF in our model). The consequence of this anticyclonic circulation includes a weaker South Equatorial Current (of the Indian Ocean) and Agulhas Current and a stronger East Australian Current (EAC). The southward flowing Leeuwin Current is also weaker in the top 100 m without ITF (not shown). However, this is compensated by a weaker northward flow at depth and so the change in depth-integrated transport is small.

Note that the difference in depth-averaged transport in the Eulerian frame does not necessarily reflect the Lagrangian pathways of water parcels. For example, the loop of circulation difference in Fig. 7c does not indicate that ITF water exiting from the southern Indian Ocean goes around southern Australia, travels north along the east coast of Australia against the EAC, and wraps around Papua New Guinea to enter the ITF channel directly. In fact, we examined the velocity fields for both open and closed ITF and found no evidence of water at any depth going against the EAC. However, the -10 Sv contour line in the transport stream function for the open case (Fig. 7a) is indicative of the path of the source water (despite the depth average). Water originating in the southern subtropical gyre (to as far south as New Zealand) goes around the gyre to the western boundary. They then turn northward along the path of the New Guinea Coastal Undercurrent (NGCUC), cross the equator into the North Pacific, zigzag their way across the North Equatorial Countercurrent (NECC) to join the North Equatorial Current (NEC), then turn southward along the path of the Mindanao Current and enter the ITF channel. This is consistent with the picture depicted by Godfrey et al. (1993) and Godfrey and Wilkin (1995) about the South Pacific origin of ITF water and its “appearance” of North Pacific origin. Gordon (1995) argued that the property of water coming from the South Pacific was modified so significantly that it was no longer appropriate to regard it as the source water of ITF.

A quantity is defined to illustrate the ITF effect on the meridional overturning circulation in the South Pacific,

$$\phi(y, z) = \int_z^0 \int_{x_w(y)}^{x_e(y)} v(x, y, z) dx dz,$$

where x , y , and z denote longitude, latitude, and depth; $x_w(y)$ and $x_e(y)$ are longitudes of western and eastern boundaries at latitude y ; $v(x, y, z)$ is meridional velocity; and $\phi(y, z)$ is the meridional transport streamfunction only if the net volume transport across a zonal section is zero: ϕ in the South Pacific with and without the ITF and their difference are presented in Fig. 8. Arrows along the contours indicate the directions of the meridional overturning circulation. To provide a better visualization of upper ocean circulation, a nonlinear scale is used for the vertical coordinate (square root of depth). For the case with ITF, the value of ϕ contains the mean ITF transport.

The shallow overturning cell is an important indicator of tropical–subtropical exchange (Lu and McCreary 1995; Lu et al. 1998). The upper part of this cell is practically unchanged (<2 Sv) with and without ITF. However, the difference begins to occur in the lower part of the cell slightly above the thermocline. The near-horizontal lines from about 80 m to about 2500 m reflects the mean ITF transport. The change in meridional flow is concentrated near the western boundary (not shown), as expected, because the two experiments have identical wind and so the same Sverdrup interior flow. Approximately 11 Sv of the difference in meridional transport occurs above the maximum ITF sill depth of 1520 m. The 2 Sv or so meridional transport below this depth reflects the depth change of a small portion of flow that goes through en-route around Australia. South of 40°S, this small transport is contributed by flow south of Tasmania and New Zealand (confirmed by velocity fields at depths between 2200 and 2500 m, not shown). A similar analysis is also performed for the Indian Ocean. The difference “streamlines” are more shallowly confined because ITF water enters the Indian Ocean at a much shallower depth than Southern Ocean water entering the Pacific.

An important effect not discussed by HG is the role of the ITF on the NGCUC, the low-latitude western boundary current (LLWBC) in the South Pacific (near 5°–10°S, 152°–155°E). Zonal sections of meridional velocity across this current at 10° S with and without the ITF and their difference are shown in Figs. 9a–c. The change in meridional velocity, although having a barotropic component, is depth-dependent. The largest change occurs at the core of NGCUC (centered at the depth of approximately 150 m), with a 40%–50% reduction in core speed. This current is an important carrier of thermocline water from the southern subtropical gyre in the Pacific to the equatorial Pacific. The absence of the ITF thus reduces tropical–subtropical exchange in the South Pacific.

In contrast, the LLWBC in the North Pacific, the Mindanao Current, is not sensitive to the ITF (Figs. 9c–e) despite the fact that much of the ITF waters come directly from the Mindanao Current. This is because the wind-driven North

Equatorial Current, the bifurcation of which feeds the Mindanao Current, should not be sensitive to the ITF that is far downstream of it. Although the ITF does not affect the Mindanao Current, it drains much of the North Pacific thermocline water carried by this current into the Indian Ocean and thus reduces the exchange between the tropical Pacific and the northern subtropical gyre.

Tropical–subtropical exchange has been investigated in several studies using simulated water parcel trajectories ([Liu and Philander 1994, 2000](#)). However, the analyses were based on models without an ITF. In the present study, a similar analysis is performed using velocity fields with and without an ITF. Similar to [Liu and Philander \(2000\)](#), water parcels are initially released at 24°N and 24°S at 50 m. These latitudes are close to the outcrop latitudes for tropical thermocline (i.e., where tropical thermocline water is ventilated). The depth of 50 m is used to represent the base of the mixed layer approximately. The parcels are advected by time-mean velocity fields (with and without ITF) for a period of 9 years. [Figure 10](#) shows the trajectories of parcels that arrive at the Tropics. They are referred to as the exchanged parcels (“exchanged” in the sense of subtropical–tropical exchange). Trajectories of parcels recirculating within the subtropical gyres (recirculated parcels) are shown in [Fig. 11](#). The color of a trajectory segment indicates the depth of the particle. In both hemispheres, the parcels roughly follow the thermocline en-route to the Tropics. Those that arrive at the equatorial Pacific eventually upwell to the surface and travel poleward following the Ekman flows.

In the presence of the ITF, many exchanged parcels from the North Pacific ([Fig. 11a](#)) that travel along the western boundary are split into two branches: one that turns eastward into the EUC and another that goes into the Indian Ocean. Blockage of the ITF causes the latter branch to join the EUC ([Fig. 11b](#)). In the South Pacific, with ITF open, parcels carried by the NGCUC cross the equator and go around the Halmahera Eddy before turning east into the equatorial Pacific ([Fig. 11c](#)). When the ITF is blocked, they are confined to the southern hemisphere and join the EUC directly. Blockage of the ITF also reduces the zonal extent of the “exchange window” within which subducted parcels can arrive at the Tropics (east of 127° and 110°W at 24°S with and without ITF, respectively). The above results suggest that the contribution of North and South Pacific thermocline waters to EUC waters would be different with and without an ITF, consistent with the finding of [Rodgers et al. \(1999\)](#).

Parcels originating between 127° and 110°W at 24°S, capable of arriving at the Tropics when the ITF is open, recirculate within the subtropical gyre when the ITF is closed ([Figs. 11c,d](#)). The excess recirculated parcels turn southeastward at the western boundary between 10° and 20°S, travel down the Australian coast and reach as far as 40°S. This is 5° farther south compared to the southern limit of the recirculated paths when the ITF is open. These parcels, after shoaling to the surface, turn northeastward and flow north of New Zealand. Consistently, analysis of the Eulerian velocity field also reveals a loop of circulation difference with and without the ITF southeast of Australia. As one of the reviewers pointed out, this difference in the recirculated trajectories off the southeast coast of Australia indicates that the ITF indirectly affects the regional climate near southeast Australia: the farther penetration of recirculated water could affect air–sea local interaction and shift the latitude of storm tracks by hundreds of kilometers.

In summary, the ITF regulates the relative magnitudes of tropical–subtropical exchanges in the Northern and Southern Hemispheres: its presence reduces (enhances) the influence of the northern (southern) subtropical gyre and thus contributes to the maintenance of the tropical thermocline property. Models that do not account for the ITF would exaggerate the effect of the northern Pacific and underestimate the role of the southern Pacific. Tropical–subtropical exchange rates inferred from such models are subject to biases due to the missing ITF effect. The water parcel trajectories without an ITF are qualitatively similar to those presented by [Liu and Philander \(2000\)](#) using velocities from a regional model that has no ITF. The difference from trajectories with an ITF clearly shows the impact of the ITF regulating the exchange and recirculation processes.


Response of circulation in the tropical Pacific is more baroclinic and so cannot be revealed by the depth-integrated flow shown in [Fig. 7](#). The difference in zonal flow in the equatorial region without and with an ITF ([Fig. 12a](#)) is characterized by eastward tendency near the surface and in the EUC (east of the date line) and westward tendency in between. Such a layer structure continues at greater depth, reflecting the highly baroclinic nature of equatorial flow. The change in vertical velocity in this region ([Fig. 12b](#)) shows a general downwelling tendency (reduced equatorial upwelling). The magnitude of the change in the eastern equatorial Pacific is about 10%–15% of the mean equatorial upwelling in the area. The change of zonal flow away from the equator (not shown) is less baroclinic, with an eastward tendency from and above the thermocline and small westward tendency at depth.


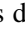
[Figure 13](#) shows the difference in horizontal velocities without and with ITF at 5 m and near the thermocline (at the depth of the 20°C isotherm). The length of arrows have been scaled by the square root of velocity magnitude to provide a better visualization of small vectors. However, the direction of the velocity vectors (i.e., ratio of zonal and meridional velocities) are preserved. The vectors are mapped from the original grid to a reduced 3° × 1° grid to avoid overlap of arrows. Several features are common for both depths: 1) a general eastward tendency is seen over most of the Pacific 2) the eastward flow turns poleward near the eastern boundary, and 3) there is a convergence of flow towards the equator. These flow patterns help to understand the change in thermal structure to be discussed later.


Hirst and Godfrey reported a “two-layer” adjustment of tropical Pacific circulation with eastward and westward




tendencies above and below 500 m when the ITF is closed and with downwelling connecting the two (their Fig. 21 with the sign reversed because it is closed–open). Our findings are similar to theirs in terms of the general eastward tendency in the upper tropical Pacific. However, the highly baroclinic adjustment of zonal flow near the equator found in our model was not shown by [HG](#).

2) MEAN THERMAL STRUCTURE


The change of circulation due to blockage of the ITF has widespread influence on subsurface temperature, most notably in the tropical Pacific and southern Indian Ocean ([Fig. 14](#) ). The general warming of the tropical Pacific and cooling of the Indian Ocean is because of the fact that the heat transport between the Pacific and Indian Ocean is cut off [approximately 0.6 PW (1 PW = 10^{15} W)].



The warming in the tropical Pacific is consistent with the general eastward tendency of horizontal velocity which turns poleward near the eastern tropical Pacific as discussed earlier (cf. [Fig. 13](#) ). Such a tendency advects warmer waters in the western tropical Pacific towards the east and spreads them poleward in the eastern tropical Pacific. Changes in temperature and horizontal velocity are consistent with geostrophic balance because the decrease in temperature away from the equator corresponds to a decrease in dynamic height and thus an eastward flow. At the equator, the downwelling tendency ([Fig. 12b](#) ) also helps depress isotherms and create warming at a given depth. The very large change near the EAC and smaller change near the Kuroshio are because of shifts in turning latitudes of these currents: the EAC extends farther south and the Kuroshio not as far north. In the Indian Ocean, the general cooling is due to the reduced heat advection from the Pacific. The larger cooling in the southern Indian Ocean is due to the weaker SEC, Agulhas Current, and Leeuwin Current, and the reduced difference of horizontal temperature between the ITF channel and these areas.

In most areas, the change in subsurface temperature is generally larger than that in the surface. Consequently, the mean thermocline depth is depressed and raised in the tropical Pacific and Indian Ocean, respectively. This is illustrated in [Fig. 15](#)  by the depth of the 20°C isotherm, D20 (a proxy for thermocline depth in the Tropics). The difference between the depths of thermocline and pycnocline due to salinity effect is small (see [appendix B](#)). The change in thermocline depth is largest in the southern Indian Ocean and the eastern equatorial Pacific. That for the latter region is substantial considering the shallowness of thermocline there.

The role of change in circulation on thermocline depth in the equatorial Pacific is illustrated in the following. The contribution by zonal, vertical, and total advection to temperature change is presented in [Figs. 16a–c](#) . They have been converted from tendency unit (°C/s) to temperature unit (°C) through the multiplication with the number of seconds in a year. They represent various contributions to temperature difference over a year (averaged over the 18-yr period). Meridional advection is relatively small near the equatorial thermocline and is thus not shown. The thick solid and dashed curves indicate the mean depths of thermocline with and without an ITF. The tendency is consistent with velocity difference (e.g., [Fig. 12](#) ) , which advects temperature downgradient (eastward and downward) to create warming at the depth of the original thermocline (namely, a deeper thermocline). The effect of vertical advection dominates in the eastern equatorial Pacific where the thermocline deepens the most. The pattern of the advective contribution is qualitatively consistent with the actual temperature difference ([Fig. 16d](#) ) in terms of the sign and the location of maximum change. However, the magnitude is much larger than the actual temperature change, reflecting the counteracting role of diffusion to maintain the actual temperature change. The effect of diffusion cannot be evaluated directly due to incomplete model output for mixing coefficients.

Mean thermocline depth reflects heat content and is widely considered to be an important precondition for longer term variation of ENSO behavior. Changes in the mean depth or property of the thermocline in the equatorial Pacific by anomalous water mass originating in the subtropics was hypothesized to cause decadal variations in ENSO behavior (e.g., [Deser et al. 1996](#); [Gu and Philander 1997](#)). Decadal changes of dominant frequency and magnitude of interannual variations due to difference in mean slope and depth of the thermocline have been demonstrated by relatively simple coupled ocean–atmosphere models of the tropical Pacific ([Kirtman and Schopf 1998](#); [Fedorov and Philander 2001](#)). The contribution of ITF to the maintenance of thermocline structure thus implicates its potential role in ENSO.

The ITF could affect the coupled ocean–atmosphere system more directly through its effect on SST. [Figure 17](#)  shows the time-mean SST with and without the ITF and their difference. Blockage of ITF results in 1) warmer equatorial SST in the central to eastern Pacific, and thus a reduced SST gradient between the warm pool and the cold tongue, and 2) a general cooling of the southern Indian Ocean south of the SEC, west of the Leeuwin Current and near the Agulhas retroflection region.

The change in the southern Indian Ocean resembles the pattern of change in subsurface temperature presented in [Fig. 14](#) . In contrast, the surface warming in the central to eastern equatorial Pacific and off the South American coast is different from the pattern of subsurface warming. This suggests different processes causing the SST differences in the two oceans. Relative contributions by various processes to the SST difference is shown in [Fig. 18](#) . The surface heat flux contribution is due to the difference in the relaxation part of the heat flux (the imposed part of the heat flux is identical with

and without an ITF). Due to incomplete output for diffusion coefficients, the effect of diffusion cannot be computed directly. We therefore obtain it by removing the effect of advection and surface heat flux from the SST difference.

In the tropical Pacific, zonal advection is important in the central equatorial Pacific (eastward spreading of warm-pool water) and off the South American coast. Meridional advection is dominant in the eastern equatorial Pacific off the equator (convergence of warmer off-equatorial water into the cold tongue). Vertical advection is large only in a narrow equatorial band in the east (downwelling of warm surface water). Total advection is as important as and counteracts surface heat flux over the central to western equatorial Pacific. Diffusion, which is large over the central to eastern equatorial Pacific, has an overall warming effect. Overall, the primary balance is between advection and surface heat flux, with secondary contribution by diffusion. In contrast, the role of advection for SST difference in the Indian Ocean is relatively small. The dominant balance is between diffusion and surface heat flux.

The pattern of SST response to the ITF and the dominant causes are similar to those presented by [HG](#) for the Indian Ocean and western Pacific (their [Figs. 13d and 16](#)). Their Fig. 13b is shown up to to 160°W only. Near that longitude, SST difference in our model is close to 0.5°C whereas it is only 0.25°C in [HG](#). Judging from the difference in surface heat flux with and without ITF presented by [HG](#) (their Fig. 1b), the maximum SST difference in the eastern equatorial Pacific (not presented) appears to be about 0.5°C, which is smaller than the 1°C difference seen in our model. The larger response of SST to ITF in the equatorial Pacific in our study is probably due to the finer resolution (both meridionally and vertically) and more sophisticated mixing schemes in our model, both of them are important to the simulation of tropical circulation and thermal structure (especially the EUC).

Similar to our model, up to 1°C warming in the central to eastern equatorial Pacific due to blockage of ITF was also reported by [Murtugudde et al. \(1998\)](#) and [Rodgers et al. \(1999\)](#), both having finer resolutions and more advanced mixing schemes than [HG](#). However, that in Murtugudde et al. has a maximum magnitude between 140° and 110°W along the equator (their Fig. 10) whereas that in Rodgers et al. is the largest off the South American coast (their Fig. 13). The warming pattern we found has local maxima in both of these areas. There are also other differences between ours and previously reported SST responses. For instance, the change of tropical SST in our model is more confined to the equatorial region than that reported by Murtugudde et al.; we do not find the large changes in SST in the interior of the South Pacific (up to 0.6°C) and northeast Pacific (over 1°) reported by Rodgers et al. SST difference is only a small residual of the large contribution by various processes. Minor differences in the contribution by individual processes can easily account for the differences in SST response to ITF among different models. Since heat balance analyses were not presented by Murtugudde et al. and Rodgers et al., we are not able to pinpoint the cause of the differences.

b. Effects on seasonal–interannual variability

1) THERMOCLINE DEPTH VARIABILITY

[Figures 19a and 19b](#) illustrate the rms variation of D20 with the Indonesian passages open and closed for timescales longer than 1.5 yr (contributed primarily by interannual signals). The difference between the two is shown in [Fig. 19c](#) (the difference between rms variation of D20, not the rms variation of the difference in D20). The interannual variability in thermocline depth in the eastern equatorial Pacific (Niño-3 area) is smaller without an ITF. This can be explained in terms of a deeper thermocline experiencing smaller depth variations in response to the same magnitude of Ekman pumping (wind forcing is identical for both model runs). In contrast to the Pacific, the interannual variability of thermocline depth in the southern tropical Indian Ocean is generally larger with blockage of the ITF due to a shallower rather than deeper thermocline. These changes suggest that local Ekman pumping is the dominant mechanism controlling interannual variations of thermocline depth in the tropical Pacific and Indian Oceans.

The rms variability for the annual band is presented in [Fig. 20](#) in a way similar to the interannual band discussed above. There are two local maxima of thermocline variability in the southern tropical Indian Ocean (10°S, 60° and 90°E). The presence of these two local maxima have been captured by XBT data ([Masumoto and Meyers 1998](#)). The amplitude of these two maxima in the model (approximately 15 m) is smaller that shown by [Masumoto and Meyers \(1998\)](#), 20–30 m. Both maxima have a clear signature in sea level data (e.g., Geosat data shown by [Perigaud and Delecluse 1992](#), TOPEX/Poseidon data shown by [Fu and Smith 1996](#)).

[Perigaud and Delecluse \(1992\)](#) suggested that annual Rossby waves contribute to these variations, but did not explain why there were local maxima in midocean. [Masumoto and Meyers \(1998\)](#) argued that the two maxima were the result of zonal variation in the strength of Ekman pumping and the resultant Rossby waves. [Wang et al. \(2001\)](#) suggested that the superposition of basin-scale “local response” to zonal mean Ekman pumping (standing waves) and Rossby waves forced by zonal anomaly of Ekman pumping (propagating waves) could explain the two local maxima and the minimum in between.

The magnitudes of these two maxima in D20 are reduced when ITF is blocked, with the reduction being more pronounced northeast of Madagascar. We have also examined seasonal variabilities in model sea level with and without an ITF and found the same behavior. The weakening of seasonal variation is opposite to that for interannual signals in the same

region, which is enhanced when the ITF is blocked. This difference indicates that local Ekman pumping, which controls the interannual variability, is not necessarily the dominant maintenance mechanism for the annual variation (otherwise the variability should increase like the interannual signals). Two other mechanisms could be at work: 1) radiation of planetary waves originating from the throughflow area (locally generated or transmitted from the Pacific) and 2) advection of planetary waves by the SEC of which strength and potential vorticity structure depends on the ITF heavily. Both of these would affect the superposition of propagating and standing waves and thus modify the magnitude and location of the maxima (and minima for that matter). Either way, it reflects the contribution of the ITF to annual thermocline variability in the southern Indian Ocean. An effort is being made to isolate the relative contribution of these two effects. The results will be reported in a separate paper.

In addition to the effects on the magnitude of thermocline depth variation, the ITF also affects the location of maximum thermocline variability at different timescales. For the annual band, the locations of the two maxima in the southern tropical Indian Ocean are shifted eastward when the ITF is blocked, resulting in a dipole pattern in the difference associated with each local maximum (Fig. 20c). In the eastern equatorial Pacific, the pool of maximum variability is also shifted eastward both for the annual and interannual bands, leaving dipolelike patterns in the difference in rms variation. These shifts imply that waves reflected from the Pacific side of the Indonesian archipelago (equatorial Kelvin waves) and those transmitted through the Indonesian seas or generated on the Indian Ocean side of the Indonesian coast (Rossby waves) could affect the locations of maximum thermocline variability (as well as the magnitude of the variability as discussed earlier).

2) SST VARIABILITY

The interannual SST variability with and without an ITF and their difference are shown in Fig. 21. The magnitude of rms variability in the central to eastern equatorial Pacific becomes smaller when the ITF is blocked. The maximum reduction is about 0.2°C , close to 15% of the total. The opposite is true for the tropical Indian Ocean but with a larger magnitude. These changes can be explained by the ITF-induced change in thermocline depth: a deeper thermocline (as well as an isotherm above the thermocline) would reduce the influence of subsurface temperature on SST in response to Ekman pumping, and vice versa. Therefore, the ITF not only affects the mean SST, but its interannual variability as well. In our model, relaxation of SST would reduce the difference with and without the ITF. The impact of the ITF on the interannual variability in coupled ocean-atmosphere models remains to be investigated.

Murtugudde et al. (1998) found that the difference in the Niño-3 index of interannual SST anomaly with and without the ITF is correlated with the Niño-3 index itself. The same is true for the Niño-4 index. No interpretation was offered for this correlation. We performed a similar analysis and found a very similar correlation. Our result offers a simple explanation. The blocking of the ITF reduces the magnitude of interannual SST anomaly in the central to eastern equatorial Pacific. Therefore, a warm (cold) event would be not as warm (cold), and thus the correlation between Niño index and the difference of the Niño indices with and without an ITF.

The largest response of interannual SST to blockage of the ITF occurs downstream of the EAC off the southeast corner of Australia. The location of maximum interannual variability is shifted from east to south of Tasmania. This is due to the strengthening of the EAC, which allows it to extend farther downstream as discussed earlier. In addition, the magnitude of interannual variability becomes twice as large (0.5° vs 1°C) when the ITF is blocked. The lack of interannual variability along the EAC when the ITF is present is consistent with the finding of Ridgway and Godfrey (1994) based on hydrographic data. The enhancement of interannual variability and the change of mean SST near the EAC discussed earlier (cf. Fig. 14), both being the largest geographically, imply that the ITF has an important contribution to the regional climate near southeastern Australia.

5. Summary and conclusions

A near-global OGCM is used to investigate effects of the ITF on the circulation and thermal structure of the Pacific and Indian Oceans. Model solutions over the period from 1981 to 1997 with open and closed Indonesian passages are compared to highlight the effects on mean state and seasonal-to-interannual variability. The model employs advanced mixing schemes and has overall higher meridional and vertical resolutions than those used in previous studies. The time period of study is also the longest and includes the most recent El Niño event.

The ITF is found to affect the loop of circulation around East Australia and the southern Indian Ocean. In particular, absence of the ITF weakens the Indian Ocean SEC and Agulhas Current and strengthens the East Australian Current. The southward flowing Leeuwin Current is also weaker in the upper 100 m without the ITF, accompanied by weaker northward subsurface flows. The response of circulation in the tropical Pacific to blockage of the ITF is characterized by 1) a general eastward flow off the equator above the thermocline, 2) highly baroclinic flows near the equator with eastward flows near the surface and along the EUC but westward flow between the surface and the EUC and below the EUC, and 3) downwelling along the equator.

The ITF does not affect the low-latitude western boundary current in the north Pacific (the Mindanao Current), but it

drains the North Pacific thermocline water carried by this current into the Indian Ocean. This reduces the tropical–subtropical exchange in the North Pacific. Meanwhile, the ITF helps maintain a stronger low-latitude western boundary current in the South Pacific (NGCUC), and thus enhances tropical–subtropical exchange of thermocline water in the South Pacific. Simulation of the trajectories of water parcels initially subducted at midlatitudes indicate that waters parcels carried by NGCUC can cross the equator in the presence of the ITF, but are confined to the Southern Hemisphere without the ITF. The “exchange window” in which subducted water parcels can reach the Tropics is wider with than without the ITF. Some parcels of southern subtropical origin can reach the Tropics with open ITF, but recirculate within the southern subtropical gyre when the ITF is closed. These “excess” recirculated parcels reach 5° farther south along the east coast of Australia and outcrop north of Tasmania. Their effect on local SST may have an impact on the regional climate near southeast Australia through air–sea interaction, a possible remote impact of the ITF.

Blockage of the ITF cuts off the heat transport from the Pacific to the Indian Ocean. This causes an overall warming and cooling in the tropical Pacific and southern Indian Ocean, resulting in a deepening and shoaling of the thermocline in these two oceans, respectively. Meanwhile, SST is lower in the southern Indian Ocean (most notably in areas south of the Indian Ocean SEC, west of the Leeuwin Current, and near the Agulhas retroflexion region) primarily due to smaller horizontal advection of heat and mixing with cooler subsurface temperature. In the central to eastern tropical Pacific, SST is warmed by eastward spreading of warm-pool water, convergence of warmer off-equatorial water into the cold tongue, reduced equatorial upwelling of colder subsurface water, and mixing with warmer subsurface water. These effects are counteracted by surface heat loss. In the Indian Ocean, the dominant balance for the SST change is between surface heat flux and diffusion.

The ITF also affects seasonal-to-interannual variability of thermocline depth and SST in the Pacific and Indian Oceans. When the ITF is blocked, thermocline depth variabilities on seasonal and interannual time scales are both reduced in the central to eastern Pacific because the deeper thermocline attenuates fluctuations in response to local Ekman pumping. Opposite to the effect on the Pacific, interannual thermocline variation in the southern Indian Ocean is enhanced by a shallower mean thermocline due to blockage of the ITF. Seasonal thermocline variation in this area, however, is actually reduced in the absence of the ITF despite the shoaling of the thermocline. This indicates that local Ekman pumping is not necessarily the dominant mechanism controlling the seasonal variability of thermocline fluctuation in the southern Indian Ocean as previously suggested (otherwise seasonal variability would also be enhanced like the interannual variability). Radiation of planetary waves from the Indonesian Throughflow area and advection by the ITF-dependent SEC could also be important.

The ITF helps maintain the magnitude of interannual SST variability through its effect on the thermocline depth, which in turn regulates the intensity of subsurface temperature influence on SST in response to Ekman pumping. The absence of the ITF reduces the magnitude of interannual SST variation in the equatorial Pacific and enhances that in the southern Indian Ocean and south of Tasmania.

Our results indicate that the ITF may affect ENSO and its decadal modulations by affecting tropical–subtropical exchanges in both hemispheres, mean thermocline depth, SST difference between the warm pool and the cold tongue, and seasonal-to-interannual variability of thermocline and SST fluctuations. Meanwhile-our findings highlight limitations in using models without ITF for ENSO diagnostics and forecasts. Models that exclude the ITF are subject to biases in mean thermocline structure, mean zonal SST difference, and seasonal-to-interannual variabilities. Applications of Pacific-domain models that exclude the ITF to study decadal modulations of ENSO are also limited because the relative contribution of the northern and southern subtropical gyres to the tropical Pacific is not accurate (over-estimate of the exchange in the north and underestimate in the south). Our results also indicate that ITF poses a difficulty in the design of an observing system used to monitor tropical–subtropical exchanges because the highly variable ITF is needed to close the mass and heat budgets.

Acknowledgments

The research described in this paper was carried out at the Jet Propulsion Laboratory, California Institute of Technology, under a contract with the National Aeronautics and Space Administration (NASA). The supercomputer used in this investigation was provided by funding from NASA's Office of Earth Science, Aeronautics, and Space Science. The computations in this paper were performed on an SGI-2000 through the JPL Supercomputing Project.

REFERENCES

Barnier B., L. Siefridt, and P. Marchesio, 1995: Thermal forcing for a global ocean circulation model using a 3-year climatology of ECMWF analyses. *J. Mar. Syst.*, **6**, 363–380. [Find this article online](#)

Boyer T. P., and S. Levitus, 1997: Objective analysis of temperature and salinity for the world ocean on a 1/4° grid. NOAA Atlas NESDIS

da Silva A., A. C. Young, and S. Levitus, 1994: *Atlas of Surface Marine Data*. NOAA Atlas NESDIS 6, 83 pp.

Deser C., M. A. Alexander, and M. S. Timlin, 1996: Upper-ocean thermal variations in the North Pacific during 1970–1991. *J. Climate*, **9**, 1840–1855. [Find this article online](#)

Fedorov A. V., and S. G. H. Philander, 2001: A stability analysis of tropical ocean–atmosphere interactions: Bridging measurements and theory for El Niño. *J. Climate*, **14**, 3086–3101. [Find this article online](#)

Ffield A., and A. L. Gordon, 1992: Vertical mixing in the Indonesian thermocline. *J. Phys. Oceanogr.*, **22**, 184–195. [Find this article online](#)

Fu L.-L., and R. D. Smith, 1996: Global ocean circulation from satellite altimetry and high-resolution computer simulation. *Bull. Amer. Meteor. Soc.*, **77**, 2625–2636. [Find this article online](#)

Gent P., and J. McWilliams, 1990: Isopycnal mixing in ocean circulation models. *J. Phys. Oceanogr.*, **20**, 150–155. [Find this article online](#)

Godfrey J. S., 1996: The effects of the Indonesian throughflow on ocean circulation and heat exchange with the atmosphere: A review. *J. Geophys. Res.*, **101**, 12217–12237. [Find this article online](#)

Godfrey J. S., and J. L. Wilkin, 1995: Reply. *J. Phys. Oceanogr.*, **25**, 1568–1570. [Find this article online](#)

Godfrey J. S., A. C. Hirst, and J. L. Wilkin, 1993: Why does the Indonesian throughflow appear to originate from the North Pacific? *J. Phys. Oceanogr.*, **23**, 1088–1098. [Find this article online](#)

Gordon A. L., 1986: Inter-ocean exchange of thermocline water. *J. Geophys. Res.*, **91**, 5037–5046. [Find this article online](#)

Gordon A. L., 1995: When is “appearance” reality? Indonesian throughflow is primarily derived from North Pacific water masses. *J. Phys. Oceanogr.*, **25**, 1560–1567. [Find this article online](#)

Gu D., and S. G. H. Philander, 1997: Interdecadal climate fluctuations that depend on exchanges between the tropics and extratropics. *Science*, **275**, 805–807. [Find this article online](#)

Hirst A. C., and J. S. Godfrey, 1993: The role of Indonesian throughflow in a global ocean GCM. *J. Phys. Oceanogr.*, **23**, 1057–1086. [Find this article online](#)

Kalnay E., Coauthors, 1996: The NCEP/NCAR 40-Year Reanalysis Project. *Bull. Amer. Meteor. Soc.*, **77**, 437–471. [Find this article online](#)

Kirtman B., and P. S. Schopf, 1998: Decadal variation in ENSO predictability and prediction. *J. Climate*, **11**, 2804–2833. [Find this article online](#)

Large W. G., J. C. McWilliams, and S. C. Doney, 1994: Oceanic vertical mixing: A review and a model with a nonlocal boundary layer parameterization. *Rev. Geophys.*, **32**, 363–403. [Find this article online](#)

Large W. G., G. Danabasglu, and S. C. Doney, 1997: Sensitivity to surface forcing and boundary layer mixing in a global ocean model: Annual-mean climatology. *J. Phys. Oceanogr.*, **27**, 2418–2447. [Find this article online](#)

Liu Z., and S. G. H. Philander, 1994: A GCM study of tropical–extratropical upper ocean water exchange. *J. Phys. Oceanogr.*, **24**, 2606–2623. [Find this article online](#)

Liu Z., 2000: Tropical–extratropical oceanic exchange. *Ocean Circulation and Climate: Observing and Modelling the Global Ocean*, G. Siedler, J. Church, and J. Gould, Eds., AP International Geophysics Series, Vol. 77, 247–257.

Lu P., and J. P. McCreary, 1995: Influence of the ITCZ on the flow of thermocline water from the subtropical to the equatorial Pacific Ocean. *J. Phys. Oceanogr.*, **25**, 2076–2088. [Find this article online](#)

Lu P., J. P. McCreary Jr., and B. A. Klinger, 1998: Meridional circulation cells and sources of the Pacific Equatorial Undercurrent. *J. Phys. Oceanogr.*, **28**, 62–84. [Find this article online](#)

Macdonald A. M., 1998: The global ocean circulation: A hydrographic estimate and regional analysis. *Progress in Oceanography*, Vol. 41, Pergamon, 281–382.


Marshall J., A. Adcroft, C. Hill, L. Perelman, and C. Heisey, 1997a: A finite-volume, incompressible Navier–Stokes model for studies of the ocean on parallel computers. *J. Geophys. Res.*, **102**, 5753–5766. [Find this article online](#)

Marshall J., C. Hill, L. Perelman, and A. Adcroft, 1997b: Hydrostatic, quasi-hydrostatic and non-hydrostatic ocean modeling. *J. Geophys. Res.*, **102**, 5733–5752. [Find this article online](#)

- Masumoto Y., and T. Yamagata, 1996: Seasonal variations of the Indonesian throughflow in a general ocean circulation model. *J. Geophys. Res.*, **101**, 12287–12294. [Find this article online](#)
- Masumoto Y., and G. Meyers, 1998: Forced Rossby waves in the southern tropical Indian Ocean. *J. Geophys. Res.*, **103**, 27589–27602. [Find this article online](#)
- Meyers G., 1996: Variation of Indonesian throughflow and the El Niño-Southern Oscillation. *J. Geophys. Res.*, **101**, 12255–12264. [Find this article online](#)
- Murray S. P., and D. Arief, 1988: Throughflow into the Indian Ocean through the Lomok Strait, January 1985–January 1986. *Nature*, **333**, 444–447. [Find this article online](#)
- Murtugudde R., A. J. Busalacchi, and J. Beauchamp, 1998: Seasonal-to-interannual effects of the Indonesian throughflow on the tropical Indo-Pacific basin. *J. Geophys. Res.*, **103**, 21425–21441. [Find this article online](#)
- Pacanowski R. C., and S. G. H. Philander, 1981: Parameterization of vertical mixing in numerical models of the tropical oceans. *J. Phys. Oceanogr.*, **11**, 1443–1451. [Find this article online](#)
- Perigaud C., and P. Delecluse, 1992: Annual sea level variations in the tropical Indian Ocean from GEOSAT and shallow water simulations. *J. Geophys. Res.*, **97**, 20169–20179. [Find this article online](#)
- Redi M., 1982: Oceanic isopycnal mixing by coordinate rotation. *J. Phys. Oceanogr.*, **12**, 1154–1157. [Find this article online](#)
- Ridgway K. R., and J. S. Godfrey, 1994: Mass and heat budgets in the East Australian Current: A direct approach. *J. Geophys. Res.*, **99**, 3231–3248. [Find this article online](#)
- Rodgers K. B., M. A. Cane, and N. H. Naik, 1999: The role of the Indonesian throughflow in equatorial Pacific thermocline ventilation. *J. Geophys. Res.*, **104**, 20551–20570. [Find this article online](#)
- Schiller A., J. S. Godfrey, P. C. McIntosh, G. Meyers, and S. E. Wijffels, 1998: Seasonal near-surface dynamics and thermodynamics of the Indian Ocean and Indonesian throughflow in a global ocean general circulation model. *J. Phys. Oceanogr.*, **28**, 2288–2312. [Find this article online](#)
- Schneider N., 1998: Indonesian throughflow and the global climate system. *J. Climate*, **11**, 676–689. [Find this article online](#)
- Schneider N., and T. Barnett, 1997: Indonesian throughflow in a coupled general circulation model. *J. Geophys. Res.*, **102**, 12341–12358. [Find this article online](#)
- Takaki H., T. Awaji, and K. Akitomo, 1996: Tidal currents in the Indonesian Seas and their effect on transport and mixing. *J. Geophys. Res.*, **101**, 12353–12373. [Find this article online](#)
- Verschell M., J. Kindle, and J. O'Brien, 1995: Effects of Indo-Pacific throughflow on the upper tropical Pacific and Indian Oceans. *J. Geophys. Res.*, **100**, 18409–18420. [Find this article online](#)
- Wang L. P., C. J. Koblinsky, and S. Howden, 2001: Annual Rossby wave in the southern Indian Ocean: Why does it “appear” to break down in the middle ocean? *J. Phys. Oceanogr.*, **31**, 54–74. [Find this article online](#)
-

APPENDIX A

6. Vertical Structure of Mean ITF Transport

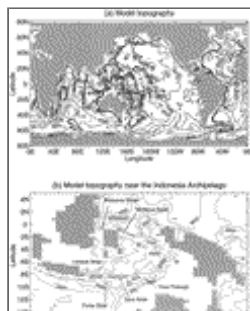
[Figure A1](#)  shows the vertical structure of the mean total ITF transport and that through various passages. The upper panel represents the transport between adjacent depth levels. The lower panel is the integration of values shown in the upper panel from the surface. ITF transport is concentrated in the upper 400 m. Below this depth, the total transport is contributed by the Timor Passage. In the lower panel, the depth where a curve turns vertical reflects the sill depth of the passage. Transport through Makassar Strait, 5.3 Sv, is weak probably due to the limited zonal resolution of the model, causing a larger proportion of the flow to go through the wider and deeper Molucca Strait to the east.

APPENDIX B

7. Difference between Thermocline and Pycnocline Depths

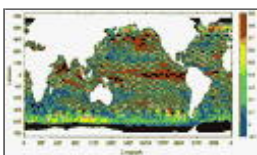
Mean potential density is calculated from the time-mean temperature and salinity over the 18-yr period (1980–97). [Figure B1](#) shows the change in depth of the mean pycnocline (defined as the surface where the mean potential density is 25) without and with an ITF. The values are very similar to the change in D20 shown in [Fig. 15](#). This suggests that the effect of salinity on the mean tropical thermocline (due to the blockage of ITF) is relatively small compared to the effect of temperature.

Figures



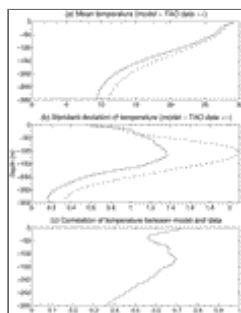
[Click on thumbnail for full-sized image.](#)

FIG. 1. Model topography (a) and its enlargement near the Indonesian archipelago (b)



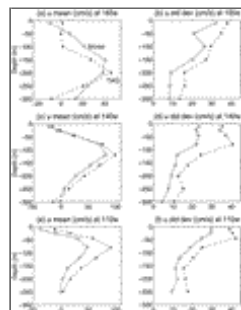
[Click on thumbnail for full-sized image.](#)

FIG. 2. Temporal correlation of sea level anomalies simulated by the model with those measured by TOPEX/Poseidon for the period of 1993–97



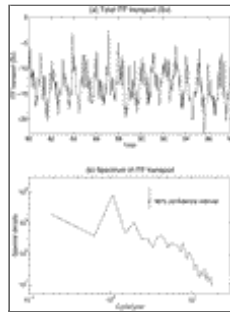
[Click on thumbnail for full-sized image.](#)

FIG. 3. Vertical profile of time-mean temperature (a) and its standard deviation (b) averaged over the 75 TOGA–TAO temperature mooring locations between 1983 and 1997 for model (solid) and TAO data (dashed) as well as the model–data correlation (c)



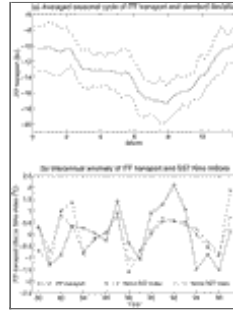
[Click on thumbnail for full-sized image.](#)

FIG. 4. Comparison of time-mean zonal velocity and its standard deviation with TAO current meter data at 165°E, 140°W, and 110°W, along the equator from 1983 to 1997



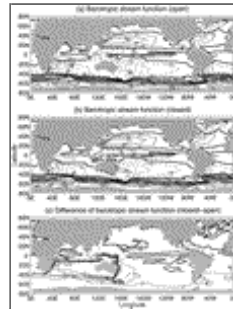
[Click on thumbnail for full-sized image.](#)

FIG. 5. Time series of the simulated total transport of the Indonesian Throughflow (a) and the corresponding frequency spectrum (b)



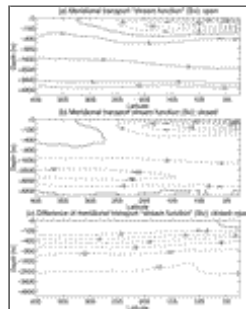
[Click on thumbnail for full-sized image.](#)

FIG. 6. The averaged seasonal cycle (a) and interannual anomaly (b) of the simulated Indonesian throughflow along with Niño-3 and Niño-4 SST indices. The dashed curves in (a) represent one standard deviation



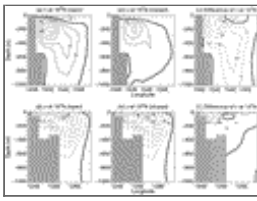
[Click on thumbnail for full-sized image.](#)

FIG. 7. Time-mean barotropic streamfunction with the Indonesian passages open (a), closed (b), and their difference (c). The unit of contour levels is Sv.



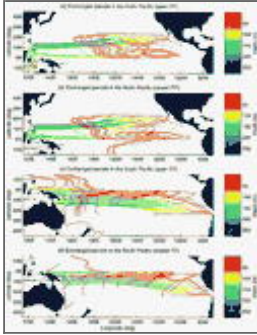
[Click on thumbnail for full-sized image.](#)

FIG. 8. Time-mean meridional transport “streamfunction” in the South Pacific with the Indonesian passages open (a), closed (b), and their difference (c)



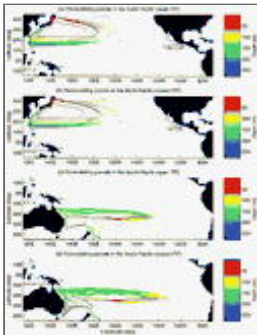
[Click on thumbnail for full-sized image.](#)

FIG. 9. Time-mean zonal sections of meridional velocities with open and closed Indonesian passages and their difference (closed-open) across the New Guinea Coastal Undercurrent (upper) and Mindanao Current (lower). (The unit of contour levels is cm s^{-1})



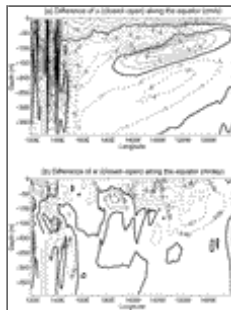
[Click on thumbnail for full-sized image.](#)

FIG. 10. Simulated trajectories of water parcels subducted in the subtropics and eventually arriving at the Tropics. Panels (a)–(d) correspond to exchanges in the North and South Pacific with and without ITF, respectively



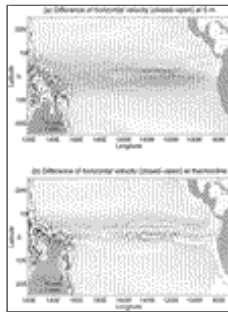
[Click on thumbnail for full-sized image.](#)

FIG. 11. Simulated trajectories of water parcels subducted in the subtropics and recirculated within the subtropical gyres. Panels (a)–(d) correspond to recirculation in the North and South Pacific with and without ITF, respectively



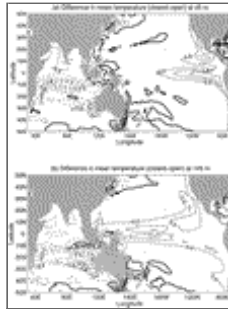
[Click on thumbnail for full-sized image.](#)

FIG. 12. Zonal sections of the difference in zonal (a) and vertical (b) velocities without and with ITF along the equator. (Units of contour levels are cm s^{-1} and m day^{-1} , respectively)



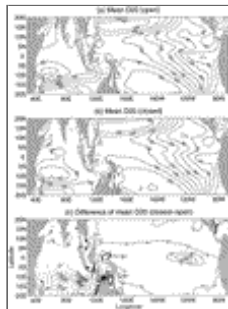
[Click on thumbnail for full-sized image.](#)

FIG. 13. Difference of horizontal velocity without and with an ITF at 5 m (a) and the thermocline (b).



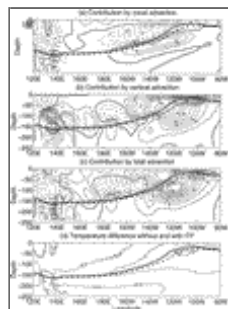
[Click on thumbnail for full-sized image.](#)

FIG. 14. Difference of temperature without and with an ITF at the depths of 50 m (a) and 150 m (b). The unit of contour levels is $^{\circ}\text{C}$



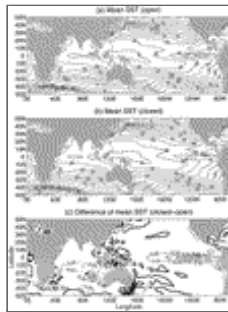
[Click on thumbnail for full-sized image.](#)

FIG. 15. Time-mean depth of the 20°C isotherm, D20, (a proxy for thermocline depth) with the Indonesian passages open (a), closed (b), and their difference (c). The unit of contour levels is the meter



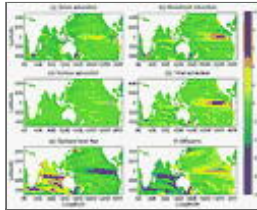
[Click on thumbnail for full-sized image.](#)

FIG. 16. Contribution of zonal (a), vertical (b), and total (c) advection to temperature difference without and with an ITF, and the actual temperature difference (d). Thick solid and dashed curves represent D20 with and without an ITF



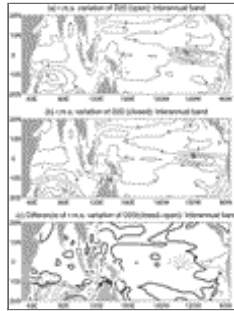
[Click on thumbnail for full-sized image.](#)

FIG. 17. Time-mean SST with the Indonesian passages open (a), closed (b), and their difference (c). The unit of contour levels is $^{\circ}\text{C}$



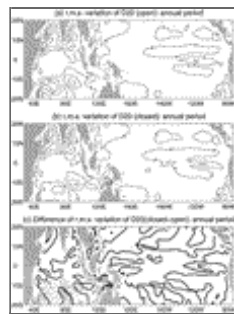
[Click on thumbnail for full-sized image.](#)

FIG. 18. Contribution of advection, surface heat flux, and diffusion to SST difference without and with an ITF



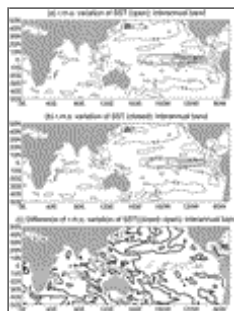
[Click on thumbnail for full-sized image.](#)

FIG. 19. Root-mean-squared variation of D20 with the Indonesian passages open (a), closed (b), and their difference (c) for interannual signals. The unit of contour levels is meter



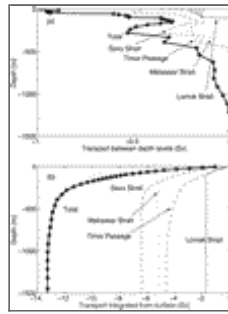
[Click on thumbnail for full-sized image.](#)

FIG. 20. Root-mean-squared variation of D20 with the Indonesian passages open (a), closed (b), and their difference (c) for the annual period. The unit of contour levels is meter



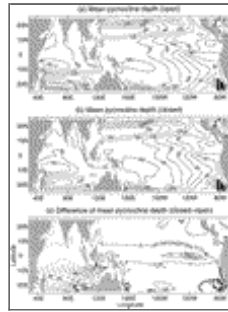
[Click on thumbnail for full-sized image.](#)

FIG. 21. Root-mean-squared variation of SST with the Indonesian passages open (a), closed (b), and their difference (c) for timescales longer than 1.5 yr (contributed primarily by interannual signals). The unit of contour levels is °C



[Click on thumbnail for full-sized image.](#)

FIG. A1. Vertical structure of transport through various passages: (a) between depth levels, and (b) integrated from the surface



[Click on thumbnail for full-sized image.](#)

FIG. B1. Depths of pycnocline (defined by the surface with potential density being 25) without (a) and with (b) an ITF and their difference (c). The values are very similar to thermocline depths and difference shown in [Fig. 15](#)

Corresponding author address: Tong Lee, Jet Propulsion Laboratory, MS 300-323, 4800 Oak Grove Drive, Pasadena, CA 91109. E-mail: tlee@pacific.jpl.nasa.gov.

[top ▲](#)



© 2008 American Meteorological Society [Privacy Policy and Disclaimer](#)
Headquarters: 45 Beacon Street Boston, MA 02108-3693
DC Office: 1120 G Street, NW, Suite 800 Washington DC, 20005-3826
amsinfo@ametsoc.org Phone: 617-227-2425 Fax: 617-742-8718
[Allen Press, Inc.](#) assists in the online publication of AMS journals.